I&EC research
Industrial & Engineering Chemistry Research

Article

pubs.acs.org/IECR

A Practical Multivariable Control Approach Based on Inverted Decoupling and Decentralized Active Disturbance Rejection Control

Li Sun,[†] Junyi Dong,[*,†] Donghai Li,[†] and Kwang Y. Lee[‡]

[†]The State Key Lab of Power Systems, Department of Thermal Engineering, Tsinghua University, Beijing 100084, PR China
[‡]Department of Electrical and Computer Engineering, Baylor University, Waco, Texas 76798-7356, United States

Supporting Information

ABSTRACT: Conventional multivariable controls may face challenges in industrial implementation due to their computation intensity, controller complexity, and/or poor robustness. To this end, this paper developed a practical multivariable control method, consisting of inverted decoupling and decentralized active disturbance rejection controller (ADRC). Strong robustness is achieved with negligible computation and simple forms of the decoupler and controller. Moreover, the disturbance rejection is markedly accelerated. On the basis of the two-input−two-output (TITO) system description, first discussed are the practical advantages of inverted decoupling that can be easily extended to high dimensional systems. Particularly, a compensation method is proposed to make the inverted decoupling applicable for the processes with right-half plane zeros. Then, the ADRC is bridged to the PI controller and the internal stability and robustness are analyzed. The feasibility of implementing ADRC in industrial distributed control system (DCS) is verified experimentally. Moreover, the qualitative tuning rules are discussed and packaged as an interactive tool. Also addressed are the compatibility and complementarity of the combination of ADRC and inverted decoupling. Finally, simulation and experimental results demonstrate the efficacy of the proposed method.

1. INTRODUCTION

Control of multivariable industrial processes becomes challenging due to the inherent interaction among variables, modeling uncertainty and various disturbances. Taking a power plant as an illustration,[1] the boiler steam pressure regulation loop is strongly impacted by the power control loop of a turbine unit. And it is difficult to derive an accurate mathematical model for the complex boiler−turbine unit. Moreover, the pressure and power are always disturbed by the variations in fuel quality. In the past 30 years, a frontier for multivariable control has been some form of model predictive control (MPC),[2] which is able to produce satisfactory performance by solving a constrained optimization problem. However, the computational intensity has limited its wide application in practice. It is only suitable for a few critical loops where the resulting benefits justify the expenditure and additional hardware costs.

Another multivariable solution is about the centralized control design in frequency domain. Skogestad and Postlethwaite[3] gave a detailed step-by-step design procedure to derive a robust optimal controller based on $\mathcal{H}_2$ and $\mathcal{H}_\infty$ norms. However, suitable weighting functions need to be determined prior to $\mathcal{H}_2$ or $\mathcal{H}_\infty$ controller design, which is often troublesome for the field engineers. Along this line, Liu and Zhang et al.[4−6] made significant development by quantitatively deriving a robust $\mathcal{H}_2$ optimal controller, which simply requires designers to assign a desired closed-loop transfer matrix instead of the obscure weighting functions. In their control scheme, all aforementioned problems, i.e., interaction, uncertainty, and disturbances, are well addressed. Moreover, intuitive tuning rules are given for online parameter adjustment in order to balance the performance and robustness. The only concern for this centralized scheme is that the controller may be of high order and even contain time-delay terms in the denominator, requiring special care for industrial implementation.

As an alternative, the combination of a fixed decoupler and decentralized controllers, originally appearing in some early references,[7−9] is promising for application due to its computational simplicity and easier online retuning. The conventional decouplers $D(s)$, such as ideal decoupling and simplified decoupling,[10] are usually derived by computing the inverse of the transfer matrix $G(s)$, that is, $D(s) = G^{-1}(s)T(s)$, where $T(s)$ is the desired decoupled matrix or namely apparent process. However, the inverse computation brings inevitable complexity either in the decoupler $D(s)$ or in the apparent process $T(s)$. For example, the ideal decoupling simply adopts the diagonal elements of the system transfer matrix $G(s)$ as the apparent process $T(s)$, which results in a complex or even physically unrealizable decoupler $D(s)$. Contrarily, the simplified decoupling scheme utilizes a simple decoupler form but puts complexity into the apparent process. Along this line there are some recent attempts to reduce complexities based on an adjoint transfer function[11] or inversion approximation.[12] Besides complexity, the inversion-based conventional decouplers may malfunction in case of actuator windup.

Different from the inversion computation, Shinskey[13] proposed an inverted decoupling method based on the concept of feed-forward compensation, which simultaneously obtains the same

Received: October 6, 2015
Revised: January 12, 2016
Accepted: January 17, 2016
Published: January 18, 2016

DOI: 10.1021/acs.iecr.5b03738
Ind. Eng. Chem. Res. 2016, 55, 2008−2019

simple apparent process $T(s)$ as the ideal decoupling and the same simple decoupler $D(s)$ as simplified decoupling. Unfortunately, this method has been ignored for a long time until Wade[14] picked it up, stressing that this technique should not be disregarded. Later, some recent research[15−20] was carried out to show the practical advantages, to address the physical realization issues, and to extend its applicability to more complex systems. Actually, the aforementioned literature[13−20] almost constitutes the complete set of open publications related to inverted decoupling in the past decades.

Although it promises computational simplicity, decoupling efficiency and easier implementation, inverted decoupling has the potential risk of poor robustness, which is inherited from the feedforward compensation. Moreover, it should be pointed out that disturbance rejection, which should be of primary concern for process control,[21] is seldom considered in both conventional and inverted decoupling research. In this paper, the two issues will be handled by moving the focus from the decoupler design to the decentralized controller design. It is natural to handle in this direction since the uncertainties and disturbances are more likely to be attenuated by advanced controller rather than by decoupling.[22]

Active disturbance rejection control (ADRC), originally proposed by Han,[23] was considered as a robust control method for single-loop processes.[24,25] By treating the disturbances and uncertainties in a unified framework, ADRC finds many successful practical applications in motion controls.[26−28] This paper will demonstrate its efficacy in process control based on an industrial distributed control system (DCS) platform and then discuss the nice compatibility of ADRC and inverted decoupling.

This paper attempts to address the aforementioned multivariable control challenges in a unified framework consisting of inverted decoupling and ADRC. The contribution of this paper is stated as follows:

(i) A practical multivariable control approach is given, which simultaneously possesses the virtues of efficient decoupling, low computation intensity, ease of implementation, strong robustness, and disturbance rejection ability.
(ii) The merits of inverted decoupling in terms of practical application are well clarified by comparison with conventional decouplers from a perspective of equations solving.
(iii) The first-order ADRC is bridged to the conventional proportional−integral (PI) controller for the first time. And, the internal stability for the nominal model is analyzed.
(iv) The feasibility of ADRC in process control is confirmed experimentally in an industrial DCS and an interactive tuning tool is provided based on a robust loop-shaping method and Monto Carlo randomized tests.

The remainder of the paper is organized as follows: Section 2 briefly analyzes the practical advantages of inverted decoupling. ADRC is introduced and analyzed in section 3. The implementation issues of the combined control strategy are discussed in section 4. Extensive simulation and an experimental test are presented in section 5. Finally, concluding remarks are given in section 6.

2. OVERVIEW OF DECOUPLING CONTROLS

In this section, it is shown that, through the perspective of equation solving, many helpful insights can be obtained on the practical advantages of inverted decoupling over conventional decoupling methods.

For simplicity and without loss of generality, the discussion is carried out based on the two-input−two-output (TITO) system description, which can be extended straightforwardly to the high dimensional systems for both conventional and inverted decouplers.

2.1. Conventional Decoupling: Implicit Equation Solving. The conventional decoupling, shown in Figure 1, is

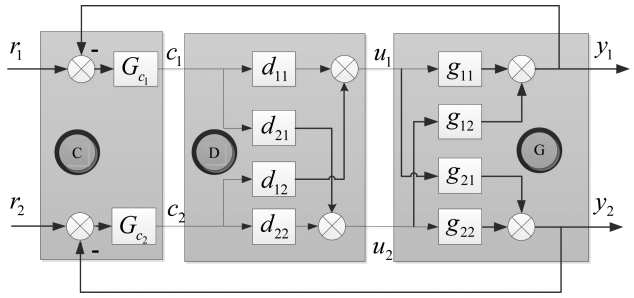

Figure 1. Conventional decoupling control system of a TITO process.

featured that the manipulated input u_i is a weighted sum of the controller outputs c_i.

The decoupled process from c_i to y_i, or namely "apparent process", is expected to be in the form of a diagonal matrix

$$T(s) = G(s)D(s) = \begin{bmatrix} T_{11}(s) & 0 \\ 0 & T_{22}(s) \end{bmatrix} \tag{1}$$

From Figure 1, (1) can be expanded in the form of algebraic equations

$$\begin{cases} d_{11}(s)g_{11}(s) + d_{21}(s)g_{12}(s) = T_{11}(s) \\ d_{11}(s)g_{21}(s) + d_{21}(s)g_{22}(s) = 0 \\ d_{22}(s)g_{12}(s) + d_{12}(s)g_{11}(s) = 0 \\ d_{22}(s)g_{22}(s) + d_{12}(s)g_{21}(s) = T_{22}(s) \end{cases} \tag{2}$$

Evidently, eqs 2 has infinite groups of possible solutions since it contains six unknowns, T_{ii} and d_{ij} but just four equality constraints. Therefore, various forms of conventional decouplers, coming from the surplus degrees of freedom, can be determined by specifying any two of the six unknown transfer functions.

Ideal Decoupling: The apparent process T_{ii} is simply set as identical to the corresponding diagonal elements of the original process, g_{ii}. Solving (1) for $D(s)$, the resulting decoupling matrix is

$$D(s) = \frac{1}{g_{11}(s)g_{22}(s) - g_{12}(s)g_{21}(s)} \begin{bmatrix} g_{22}(s)g_{11}(s) & -g_{12}(s)g_{22}(s) \\ -g_{21}(s)g_{11}(s) & g_{11}(s)g_{22}(s) \end{bmatrix} \tag{3}$$

Evidently, this decoupler is too complex to be realized. To this end, Luyben[7] proposed the simplified decoupling (abbreviated as SD hereafter) structure by specifying the diagonal elements of the decoupler as unity, which leads to a simple decoupler form

$$D(s) = \begin{bmatrix} 1 & -\dfrac{g_{12}(s)}{g_{11}(s)} \\ -\dfrac{g_{21}(s)}{g_{22}(s)} & 1 \end{bmatrix} \tag{4}$$

DOI: 10.1021/acs.iecr.5b03738
Ind. Eng. Chem. Res. 2016, 55, 2008−2019

But, the resultant apparent process is complex

$$T(s) = [g_{11}(s)g_{22}(s) - g_{12}(s)g_{21}(s)]\begin{bmatrix} \frac{1}{g_{22}(s)} & 0 \\ 0 & \frac{1}{g_{11}(s)} \end{bmatrix} \quad (5)$$

which is difficult for outer controller design.

To avoid the feasibility difficulty of simplified decoupler, Shen et al.[11] proposed an adjoint transfer matrix based decoupling (abbreviated as AD hereafter) to obtain a simple decoupler

$$D(s) = \mathrm{adj}(G(s)) = \begin{bmatrix} g_{22}(s) & -g_{12}(s) \\ -g_{21}(s) & g_{11}(s) \end{bmatrix} \quad (6)$$

but to bring a complex apparent process

$$\begin{aligned} G_a(s) &= G(s)\cdot\mathrm{adj}(G(s)) \\ &= [g_{11}(s)g_{22}(s) - g_{12}(s)g_{21}(s)]\begin{bmatrix} 1 & 0 \\ 0 & 1 \end{bmatrix} \end{aligned} \quad (7)$$

What is worse, for high dimensional systems, the decoupler simplicity of SD (4) and AD (6) does not hold at all, and the complexity of the apparent process (3), (5), and (7) grows drastically with dimension. Another shared drawback of SD and AD is that the diagonal elements of their apparent transfer functions are different from those of the original model. It implies that the controller parameters should be retuned depending on the operation modes, manual, or automatic.

Thus, it can be concluded that, under the conventional decoupling structure, the complexity cannot be avoided simultaneously at both the apparent process and decoupler, because the complexity originates from the fact that the decoupler elements can only be obtained by solving a series of algebraic equations implicitly.

2.2. Inverted Decoupling: Explicit Feedforward Compensation. Under the inverted decoupling (ID) scheme, the manipulated input (u_i) in one loop is computed by a weighted sum of its own controller output (c_i) and manipulated outputs (u_j) from other loops. For a TITO system, the structure is shown in Figure 2.

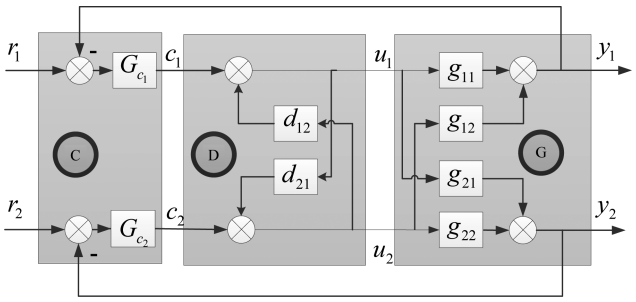

Figure 2. Inverted decoupling control system of a TITO process.

Note that in the ID scheme the interaction is actually treated as an external disturbance, which is then rejected by feedforward compensation. Thus, the decoupling elements can be obtained explicitly in terms of the process transfer functions,

$$d_{12} = -\frac{g_{12}}{g_{11}} \quad (8)$$

$$d_{21} = -\frac{g_{21}}{g_{22}} \quad (9)$$

The decoupling structure in Figure 2 can be extended to an abstract form in Figure 3 to describe general systems.

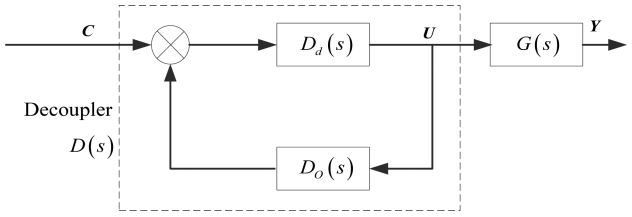

Figure 3. Equivalent matrix form for inverted decoupling.

Consider a general multivariable system of n dimensions

$$G(s) = \begin{bmatrix} g_{11}(s) & g_{12}(s) & \cdots & g_{1n}(s) \\ g_{21}(s) & g_{22}(s) & \cdots & g_{2n}(s) \\ \vdots & \vdots & \ddots & \vdots \\ g_{n1}(s) & g_{n2}(s) & \cdots & g_{nn}(s) \end{bmatrix} \quad (10)$$

and $D_d(s) = I_{n\times n}(s)$ is an all-pass path that conveys the controller output to corresponding manipulated input in the same loop. Similar to the treatment for TITO systems, the feedforward compensations for the ith manipulated input are from the other $(i-1)$ loops, which can be expressed in a matrix form

$$D_o(s) = \begin{bmatrix} 0 & -\frac{g_{12}}{g_{11}} & \cdots & -\frac{g_{1n}}{g_{11}} \\ -\frac{g_{21}}{g_{22}} & 0 & \cdots & -\frac{g_{2n}}{g_{22}} \\ \cdots & \cdots & \ddots & \cdots \\ -\frac{g_{n1}}{g_{nn}} & -\frac{g_{n2}}{g_{nn}} & \cdots & 0 \end{bmatrix} \quad (11)$$

The derivation of (11) seems quite natural and is usually referred to as an empirical feedforward compensation, which is widely used in industry. Here, it is attempted to mathematically prove that the inverted decoupling is a full decoupling method.

Theorem 1: For the inverted decoupling scheme described in Figure 3, $D_d(s) = I_{n\times n}(s)$ and $D_o(s)$ in (11), the transfer matrix of the apparent process is diagonal, shown below

$$T(s) = G(s)D(s) = \mathrm{diag}\{g_{11}(s), g_{22}(s), ..., g_{nn}(s)\} \quad (12)$$

Proof: It follows from Figure 3 that the equivalent decoupler can be expressed as

$$D(s) = D_d(s)(I - D_o(s)D_d(s))^{-1} \quad (13)$$

whose inverse is

$$D^{-1}(s) = (I - D_o(s)D_d(s))D_d^{-1}(s) = D_d^{-1}(s) - D_o(s) \quad (14)$$

Since $D_d(s) = D_d^{-1}(s) = I_{n\times n}(s)$, one obtains

$$D^{-1}(s) = \begin{bmatrix} 1 & \frac{g_{12}}{g_{11}} & \cdots & \frac{g_{1n}}{g_{11}} \\ \frac{g_{21}}{g_{22}} & 1 & \cdots & \frac{g_{2n}}{g_{22}} \\ \vdots & \cdots & \ddots & \vdots \\ \frac{g_{n1}}{g_{nn}} & \frac{g_{n2}}{g_{nn}} & \cdots & 1 \end{bmatrix} \quad (15)$$

DOI: 10.1021/acs.iecr.5b03738
Ind. Eng. Chem. Res. 2016, 55, 2008−2019

Note that there is common denominator of each row in (15). By matrix factorization, one obtains

$$D^{-1}(s) = \begin{bmatrix} g_{11}^{-1} & 0 & \cdots & 0 \\ 0 & g_{22}^{-1} & \cdots & 0 \\ \vdots & \cdots & \ddots & \vdots \\ 0 & 0 & \cdots & g_{nn}^{-1} \end{bmatrix} \begin{bmatrix} g_{11} & g_{12} & \cdots & g_{1n} \\ g_{21} & g_{22} & \cdots & g_{2n} \\ \vdots & \cdots & \ddots & \vdots \\ g_{n1} & g_{n2} & \cdots & g_{nn} \end{bmatrix} \tag{16}$$

Thus, the transfer matrix of the apparent process can be obtained as

$$\begin{aligned} T(s) &= [T^{-1}(s)]^{-1} \\ &= [D^{-1}(s)G^{-1}(s)]^{-1} \\ &= \mathrm{diag}\{g_{11}(s), g_{22}(s), ..., g_{nn}(s)\} \end{aligned} \tag{17}$$

Q.E.D. The proof shows that the inverted decoupling combines the simple parts of both ideal decoupling and simplified decoupling in that it has the same apparent process as the former and the same decoupling elements as the latter. Further merits on the inverted decoupling are summarized as follows:

(1) The computation procedures are very easy, for which even manual calculation is sufficient to derive the decoupling elements. Moreover, the extension of inverted decoupling to high dimensional systems brings no additional complexity, both in computation and decoupler form.
(2) The decoupled system has the same diagonal elements as those of the original system. It implies that the system may hold stable even if some of the decoupling elements are not yet put into "automatic" mode.
(3) The input signals to the decoupling elements can be measured directly from the actuator rather than the computed controller outputs. Each decoupled control loop is thus immune to the actuator abnormalities, e.g., windup, in other loops.
(4) Inverted decoupling can be easily configured in a DCS using the common function blocks and naturally provide the features of bumpless transfer.

2.3. Realizability and Stability. The decoupling elements in (11) may be of improper form with predicted terms, which makes it unrealizable. The improperness resulting from time delays, e.g., the time delay is smaller in g_{12} than in g_{11}, has been overcome in ref 14 by reasonable reparing or adding artificial time delay. The difficulties associated with relative degree have been addressed in ref 18 by extending the ID configurations to allow for more flexibility.

Since there exists an inner closed-loop from c_i to u_i, the decoupler may be unstable. The stability boundary was given in terms of the static relative gain of the process.[14] Later, the work[17,18] broadened the boundary by introducing unity feedback and rearranging the decoupling elements, respectively.

Another stability problem comes from the right-half plane (RHP) zeroes of the diagonal elements of the plant, leading to unstable poles in (11). To this end, some modifications[17,18] of ID are given to accommodate the cases where the RHP zeros happen to exist in all the elements of one row. In this paper, the general cases are addressed under the original ID structure based on the first-order Maclaurin series expansion,

$$e^{-\tau s} = 1 - \tau s \tag{18}$$

It is a common technique to approximate the time delay based on (18), which can usually be found in the internal model control based proportional−integral−derivative (PID) tuning and $\mathcal{H}_\infty$ synthesis. Here, (18) is used in an adverse direction to approximate the RHP zeros as a time delay term. By doing so, the realizability issue is transformed to the pairing problem, which has already been solved in ref 14.

Similar to the conventional feedforward controls, one main drawback that limits the wide application of ID pertains to its poor robustness to the modeling uncertainties. In this paper, the modeling uncertainties, including the approximation error from (18), are expected to be estimated and compensated by the ADRC, to which we turn next.

3. ACTIVE DISTURBANCE REJECTION CONTROL

To work with the inverted decoupler in industrial application, the decentralized controller is required to meet the following specifications:

(i) It should actively mitigate the effects resulting from the model mismatch in decoupler elements.
(ii) The unknown disturbances should be rejected promptly.
(iii) It should be easy for implementation and online tuning.

Active disturbance rejection control (ADRC) shows promising attributes in fulfilling the requirements above, for which many convincing cases can be found in a plenary talk.[29] In this section, the ADRC controller is articulated in a special way beginning from the description compared to to a conventional PI controller.

3.1. ADRC: An Improved Structure of a PI Controller. At present, the digital form of a PI controller is realized as a simple weighted sum of control errors. However, the historical invention of integral action is realized as a form named "automatic reset",[21] shown in Figure 4. It is seen that, in the case

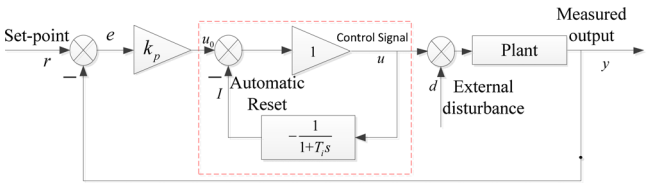

Figure 4. Implementation of integral action as automatic reset.

of a step external disturbance with magnitude d entered into the process, the automatic reset, i.e., integrator output, I, will be eventually increased by d in a passive manner. The final steady state is achieved by constantly integrating the measured errors.

Note that the automatic reset in Figure 4 only uses the information on the control signal. It is natural to revise the structure by sending more information (both control signal and measured output) to an advanced observer, with the purpose of estimating the disturbance in an active manner, which will achieve a higher efficiency than that of the automatic reset block. The observer in the modified structure, shown in Figure 5, is called an extended state observer (ESO), whose mechanism is formulated below.

For first-order ADRC design, an uncertain system with unknown order is commonly reorganized as follows[30,31]

$$\dot{y} = g(t, y, \dot{y}, ..., w) + bu \tag{19}$$

DOI: 10.1021/acs.iecr.5b03738
Ind. Eng. Chem. Res. 2016, 55, 2008−2019

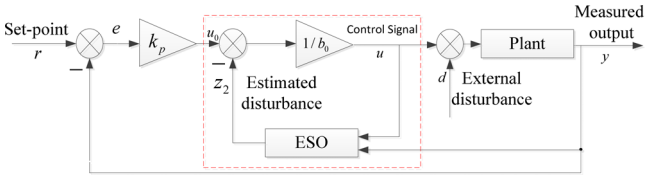

Figure 5. Modifying a PI controller as a first-order ADRC.

Where, w is the external disturbance, g denotes the system dynamics, and b is the high-frequency gain, whose accurate value is difficult to obtain. Let us rewrite (19) as

$$\dot{y} = f + b_0 u \tag{20}$$

where, b_0 is an approximate value of b and $f = g + (b - b_0)u$ is called "total disturbance", which consists of external disturbance and unknown dynamics. Consider f as an extended state and denotes $h = \dot{f}$, then (20) can be expressed in a state-space model

$$\begin{cases} \begin{bmatrix} \dot{x}_1 \\ \dot{x}_2 \end{bmatrix} = \begin{bmatrix} 0 & 1 \\ 0 & 0 \end{bmatrix} \begin{bmatrix} x_1 \\ x_2 \end{bmatrix} + \begin{bmatrix} b_0 \\ 0 \end{bmatrix} u + \begin{bmatrix} 0 \\ 1 \end{bmatrix} h \\ y = \begin{bmatrix} 1 & 0 \end{bmatrix} \begin{bmatrix} x_1 \\ x_2 \end{bmatrix} \end{cases} \tag{21}$$

for which an extended state observer (ESO) can be designed as

$$\begin{bmatrix} \dot{z}_1 \\ \dot{z}_2 \end{bmatrix} = \begin{bmatrix} -\beta_1 & 1 \\ -\beta_2 & 0 \end{bmatrix} \begin{bmatrix} z_1 \\ z_2 \end{bmatrix} + \begin{bmatrix} b_0 & \beta_1 \\ 0 & \beta_2 \end{bmatrix} \begin{bmatrix} u \\ y \end{bmatrix} \tag{22}$$

The time domain convergence of the ESO is proved based on the *state space description* in ref 32 provided that h is bounded. Gao[33] further reduced the parameters of the observer into one by introducing an observer bandwidth, ω_o, such that,

$$\beta_1 = 2\omega_o, \qquad \beta_2 = \omega_o^2 \tag{23}$$

By modifying the control signal with the estimated total disturbance in real time as

$$u = \frac{u_0 - z_2}{b_0} \tag{24}$$

the process (20) can be rewritten as

$$\dot{y} = f + b_0\left(\frac{u_0 - z_2}{b_0}\right) \approx f + b_0\left(\frac{u_0 - f}{b_0}\right) = u_0 \tag{25}$$

which shows that the effect of the total disturbance can be canceled nicely, and the resulting process, from u_0 to y, can be approximated as a simple integral process.

The approximate process (25) can be readily controlled by a proportional control

$$u_0 = k_p(r - y) \tag{26}$$

as shown in Figure 5 and the resulting closed-loop transfer function is

$$G_{cl}(s) = \frac{y(s)}{r(s)} = \frac{k_p}{s + k_p} \tag{27}$$

Note that k_p happens to be the closed-loop bandwidth, making the tuning simpler.

Although the modification from PI to first-order ADRC seems minor, the resulting robustness enhancement and performance improvement are notable, which will be shown in the next sections.

3.2. Internal Stability Analysis. Currently, with the condition of bounded h, the close-loop stability and convergence of the nth order ADRC to control an nth order system is proved in time domain,[34] where the ESO is designed by reorganizing the system in a more accurate form $y^{(n)} = g(t, y, \dot{y}, ..., y^{(n-1)}, w) + bu$ with known order. For the cases where the low-order ADRC ($n = 1$ or 2) is used to control the unknown high order systems, it is proved in ref 35 that there exists a group of parameters that can stabilize a stable plant.

In this paper we will use the first-order ADRC due to the simplicity, effectiveness, and ease of tuning.[30,31] Another motivation is that many industrial plants are difficult to accurately describe and thus usually approximated as a first-order model, based on which the *internal stability*[36] of a nominal ADRC control system will be analyzed through the classical transfer function method.

Consider a simple first-order inertia model

$$P(s) = \frac{K}{1 + Ts} \tag{28}$$

whose high-frequency gain is $b = K/T$. Noting that only positive bandwidths of ω_o and k_p are of interest in practice, we have the following theorem

Theorem 2:

(i) For a stable model ($T > 0$) given in (28), the nominal control system in Figure 5 is internally stable if and only if $\omega_o > 0$ and $k_p > 0$.

(ii) For the unstable model ($T < 0$) given in (28), the nominal control system is internally stable if and only if $\omega_o > 0, k_p > 0$, $(2k_p + \omega_o)T > -1$ and

$$2K^2\omega_o T^2(k_p + \omega_o)^2 + 2K^2\omega_o + TK^2\omega_o(4k_p + 5\omega_o) > 0 \tag{29}$$

Proof: The state space expression of ESO in (22) is first transformed into the transfer function expression

$$\begin{bmatrix} z_1(s) \\ z_2(s) \end{bmatrix} = \begin{bmatrix} \dfrac{b_0 s}{s^2 + \beta_1 s + \beta_2} & \dfrac{\beta_1 s + \beta_2}{s^2 + \beta_1 s + \beta_2} \\ \dfrac{-\beta_2 b_0}{s^2 + \beta_1 s + \beta_2} & \dfrac{\beta_2 s}{s^2 + \beta_1 s + \beta_2} \end{bmatrix} \begin{bmatrix} u(s) \\ y(s) \end{bmatrix} \tag{30}$$

Combining (20), (23), and (30) yields $z_2 = \omega_o^2/(s + \omega_o)^2 f$, implying that, in frequency domain, z_2 is actually a low-pass filtered signal of f, whose estimation accuracy is dependent on the observer bandwidth ω_o. Also it can be found that $\omega_o > 0$ is required for the stability of ESO and thus the internal stability of the whole control system.

On the basis of (30), the control structure in Figure 5 can be transformed into an equivalent structure shown in Figure 6 with tedious derivations omitted.

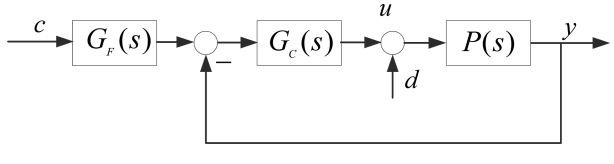

Figure 6. Equivalent ADRC structure for analysis.

DOI: 10.1021/acs.iecr.5b03738
Ind. Eng. Chem. Res. 2016, 55, 2008−2019

It is seen that ADRC is intrinsically a two-degrees-of-freedom strategy, where the feedback controller and set-point prefilter are

$$G_C(s) = \frac{k_p s^2 + (\omega_o{}^2 + 2k_p\omega_o)s + k_p\omega_o{}^2}{b_0 s(s + 2\omega_o)} \quad (31)$$

$$G_F(s) = \frac{k_p(s + \omega_o)^2}{k_p s^2 + (\omega_o{}^2 + 2k_p\omega_o)s + k_p\omega_o{}^2} \quad (32)$$

It can be first found that the ADRC controller (31)−(32) is stable if $\omega_o > 0$ and $k_p > 0$. For the nominal case of (28) where $b_0 = b = K/T$, the closed-loop characteristic equation of Figure 6 is obtained as

$$s^3 + \left(k_p + 2\omega_o + \frac{1}{T}\right)s^2 + 2\left(k_p + \frac{\omega_o}{2} + \frac{1}{T}\right)\omega_o s + k_p\omega_o{}^2 = 0 \quad (33)$$

On the basis of the Routh Criterion, the system is stable if and only if all the coefficients in (33) are positive and the following inequality exists:

$$2K^2\omega_o T^2(k_p + \omega_o)^2 + 2K^2\omega_o + TK^2\omega_o(4k_p + 5\omega_o) > 0 \quad (34)$$

Thus, we can reach Theorem 2.

Remark: It can be seen that (33) and (34) have possible solutions with $\omega_o < 0$. But it will make the ESO block unstable, thus it is dismissed from the solution set for the internal stability.

It follows from (31) that the resulting feedback controller of ADRC contains integral action, guaranteeing no steady state error in the presence of modeling uncertainties and disturbances.

3.3. Robustness. Since the nominal model (28) used for stability analysis is too simple to completely describe the industrial processes in terms of parameter uncertainty, unmodeled high order dynamics and even time delay, it is necessary to discuss the robustness of the ADRC controller. In this paper, we used the sensitivity functions and complementary sensitivity functions, respectively defined below,

$$\mathcal{S}(s) = \frac{1}{1 + G_C(s)G(s)} \quad (35)$$

$$\mathcal{T}(s) = \frac{G_C(s)G(s)}{1 + G_C(s)G(s)} \quad (36)$$

where, $G(s)$ is the plant model that can be of any form. Assuming the uncertainty is in the multiplicative form, the real plant $G'(s)$ is expressed as

$$G'(s) = G(s)(1 + \Delta(s)) \quad (37)$$

If the uncertainty $\Delta(s) \in \mathcal{H}_\infty$, the uncertain system remains stable[21] if and only if

$$|\mathcal{T}(j\omega)| \le \frac{1}{|\Delta(j\omega)|} \quad \text{for any } \omega \quad (38)$$

Evidently, it is difficult to analytically derive a robust stability region based on (38). For simplicity, the maximum sensitivity function $M_S = \|\mathcal{S}(s)\|_\infty$ and complementary sensitivity function $M_T = \|T(s)\|_\infty$ are commonly used as a numeric robustness index, whose reasonable settings are within the range $1.2 < M_T < 2.0$ and $1.4 < M_S < 2.5$.[37]

Monto Carlo randomized tests are also used in this paper to intuitively examine the performance robustness, which is shown as a quite efficient method in previous works.[38,39]

4. IMPLENTATION ISSUES OF THE COMBINED METHOD

4.1. Realizability of ADRC in Industrial DCS. The ADRC has been successfully applied in practical motion control systems. In this section, the realizability of ADRC will be tested in a DCS, which is widely utilized in the process industry. Based on the control law given in (22), (24), and (26), ADRC can be readily configured in the Ovation DCS, Emerson Process Management. The clear configuration diagram can be found in the Supporting Information. It can be seen that the diagram is a little more complex than expected because it incorporates bumpless transfer from ADRC to the PI controller or manual control. For a detailed mathematical description of bumpless transfer, the reader is referred to ref 40.

A water tank experiment is designed, as shown in Figure 7, to test the efficiency of the ADRC. The water level is controlled by the pump motor and the disturbance variable is in the outlet valve. The comparison results of ADRC and PI are shown in Figures 8 and 9.

Figure 7. Water tank control system.

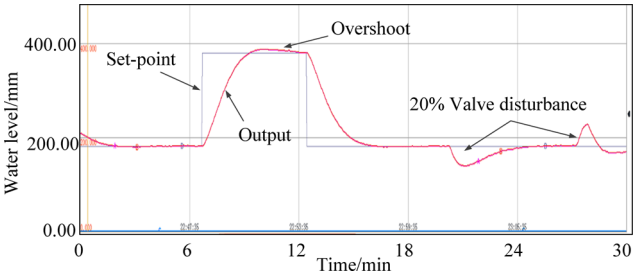

Figure 8. Responses of PI controller (the unit time scale is 6 min).

The parameters of PI are tuned by an experienced engineer and the ADRC parameters are tuned by the authors. This is simply to show that ADRC is feasible in DCS and can be quickly manually tuned without a priori detailed information on the process. This big advantage explains the dominant role that PID/PI controllers play in the industry, now shared by the ADRC. On the contrary, many advanced model-based controllers cannot be implemented without a model. Also, the results imply

DOI: 10.1021/acs.iecr.5b03738
Ind. Eng. Chem. Res. 2016, 55, 2008−2019

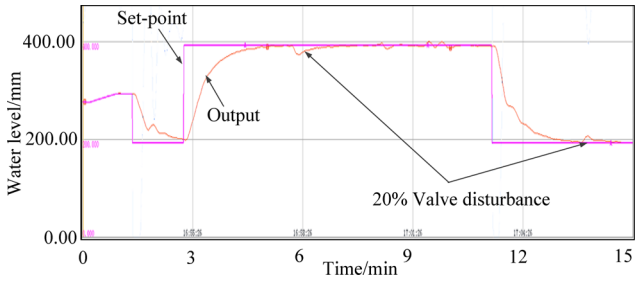

Figure 9. Responses of ADRC (the unit time scale is 3 min).

the superior performance and the robustness of ADRC, especially in disturbance rejection, which will be further demonstrated with several case studies in Section 5.

4.2. Parameter Tuning. In many cases, we can obtain a rough model about the process, which can help to obtain a set of reasonable parameters and thus improve the performance. The first-order ADRC parameters have explicit physical meaning, which makes it possible for fast online tuning. Several empirical guidelines[30] are briefly listed below:

(i) Based on (27), a larger k_p corresponds to faster tracking speed and poorer robustness.
(ii) In light of (24), a stronger control action can be obtained by increasing b_0 with the sacrifice of robustness.
(iii) A bigger observer bandwidth ω_o may result in a better robustness to the parameter uncertainties but a smaller stability margin to the unmodeled dynamics and uncertain delays.

For practical simplicity, an interactive tuning tool is developed based on MATLAB/SIMULINK [MATLAB and Simulink are registered trademarks of The MathWorks, Inc.], as shown in Figure 10. The execute file and the codes files can be downloaded

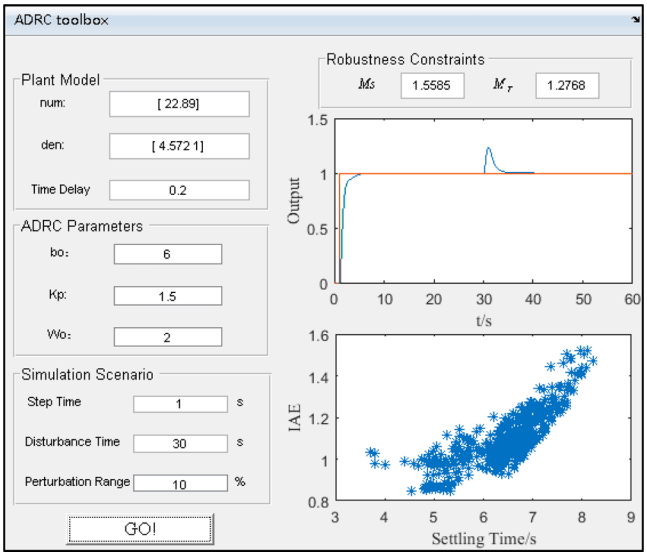

Figure 10. Interactive tuning tool for the first-order ADRC.

from the Supporting Information. One can input the model parameters and tune the parameters on the left panels of the tool. The robustness constraints $1.2 < M_T < 2.0$ and $1.4 < M_S < 2.5$ should be guaranteed while tuning. Also, the tracking and disturbance rejection performance is provided on the right panels as well as the Monte Carlo Randomized tests by perturbing the model parameters in a prescribed range.

4.3. Compatibility and Complementarity. In this section, it is established why ADRC is utilized as the decentralized controller to collaborate with inverted decoupling. In light of the remarks of inverted decoupling in section 2, the motivations are listed as follows:

(1) The ADRC can be considered as working in a model-assisted framework, where the nondiagonal transfer functions are modeled as major disturbances and rejected directly by feedforward ID compensation. Then ADRC can neglect such disturbances and is only responsible for the unmodeled dynamics and some other minor disturbances from unknown sources.
(2) For the resulting nominal SISO process from inverted decoupling, the ADRC can be designed and tuned based on the diagonal elements conveniently with the help of the toolbox.
(3) Very little complexity is added into the system by modifying the integrator of the PI controller into ESO.
(4) ADRC and inverted decoupling share a similar operating principle: disturbance measurement or estimation and active compensation.
(5) Both of them can be easily configured in a DCS and with bumpless transfer. Thus, they are perfectly compatible. Benefiting from the integral mechanism in ESO, the bumpless transfer can also be realized simply between the modes of PI control, manual control, and ADRC control.

Therefore, it is concluded that ADRC is compatible and complementary to inverted decoupling. Using ADRC as the decentralized controller, the robustness of the conventional control system can be significantly improved, which will be illustrated in the next section.

5. CASE STUDIES

In this section, five case studies are used to test the performance and robustness of the combined framework of inverted decoupling and decentralized ADRC (abbreviated as ID-ADRC). For a fair comparison, the simulation is carried out based on the benchmark models, where the parameters of most compared strategies are just transported from the public literatures without any retuning. The ADRC parameters are tuned based on the diagonal elements of the transfer matrix via the interactive tool in section 4.2.

5.1. Example 1. Consider a benchmark model of an industrial-scale polymerization reactor[41]

$$G(s) = \begin{bmatrix} \dfrac{22.89e^{-0.2s}}{4.572s+1} & \dfrac{-11.64e^{-3s}}{1.807s+1} \\ \dfrac{4.689e^{-0.2s}}{2.174s+1} & \dfrac{5.8e^{-0.4s}}{1.801s+1} \end{bmatrix} \tag{39}$$

Based on which, a centralized PI was proposed in ref 42 based on the equivalent transfer function method, and a centralized PID was proposed in ref 10 based on the concept of Nyquist set. The inverted decoupler is simply designed based on the principles in section 2. The decentralized ADRC controllers are tuned using the interactive tool with the parameters below: $b_{01} = 6$, $k_{p1} = 1.5$, $\omega_{o1} = 2$ for the first loop and $b_{02} = 6$, $k_{p2} = 2$, $\omega_{o2} = 2.5$ for second loop. Note that the tuning results of the first loop are shown in Figure 10, including the nominal performance and robustness tests. A unit step input is set for the set-points at $t = 0$ and 10 s, respectively. Step disturbances of the magnitude 0.1 are added into the two inputs at $t = 25$ s. The nominal performance is shown in

DOI: 10.1021/acs.iecr.5b03738
Ind. Eng. Chem. Res. 2016, 55, 2008−2019

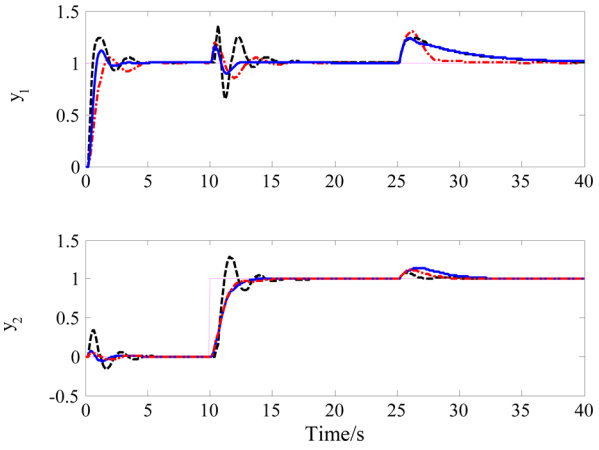

Figure 11. Tracking and disturbance rejection performance for example 1 (dotted in pink setpoint; dashed in black centralized PI; solid in blue centralized PID; dashed−dotted in red ID-ADRC).

Figure 11. It can be seen that the decoupling performance of the centralized PI control is poor. And, the centralized PID control shares similar performance with the ID-ADRC combination, but the latter produces a more prompt disturbance rejection.

Moreover, all the parameters in (39) were randomly perturbed within a range of ±10% and the previous simulation is repeated by 1000 times for the perturbed systems. Every time the integrated absolute error (IAE) and tracking overshoot for each loop are calculated in the whole 40 s. The records for every perturbed system are shown in Figure 12, where the intensive degree of the scattered points imply the strong robustness of the ID-ADRC scheme.

5.2. Example 2. Consider a binary distillation column system given by Wood and Berry[43]

$$\begin{bmatrix} y_1(s) \\ y_2(s) \end{bmatrix} = \begin{bmatrix} \dfrac{12.8e^{-s}}{16.7s+1} & \dfrac{-18.9e^{-3s}}{21s+1} \\ \dfrac{6.6e^{-7s}}{10.9s+1} & \dfrac{-19.4e^{-3s}}{14.4s+1} \end{bmatrix} \begin{bmatrix} u_1(s) \\ u_2(s) \end{bmatrix} \tag{40}$$

Various control methods are designed for this benchmark problem, such as decentralized PI control,[43] decentralized ADRC control,[44] simplified decoupling PI control (SD-PI),[45] and adjoint transfer matrix decoupling based PID control.[11] These results will be compared with the inverted decoupling based ADRC control whose parameters are, $b_{01} = 1.5$, $k_{p1} = 0.75$, $\omega_{o1} = 0.20$ for the first loop and $b_{02} = -5.0$, $k_{p2} = 0.80$, $\omega_{o2} = 0.16$ for the second loop. A unit step input is set for the set-points at $t = 0$ and 100 s, respectively. Step disturbances of the magnitude 0.1 are added into the two inputs at $t = 200$ s. The IAE for each loop is calculated in the whole process of simulation, summarized in Table 1. Selected responses are shown in Figure 13.

It is seen that the ID-ADRC scheme achieves the best decoupling, tracking, and disturbance rejection. The parameters in (40) were randomly perturbed within a range of ±10%. For all the perturbed systems, the simulation is carried out as a step input is added into the reference of the first loop. Then the performance indices, IAE = $IAE_1 + IAE_2$ and the settling time are recorded for each perturbed system, as shown in Figure 14. It can be found that the nice performance of the ID-ADRC scheme is retained to the greatest extent in the presence of the model perturbation. The intensity of the scattered points implies the strong robustness of the ID-ADRC.

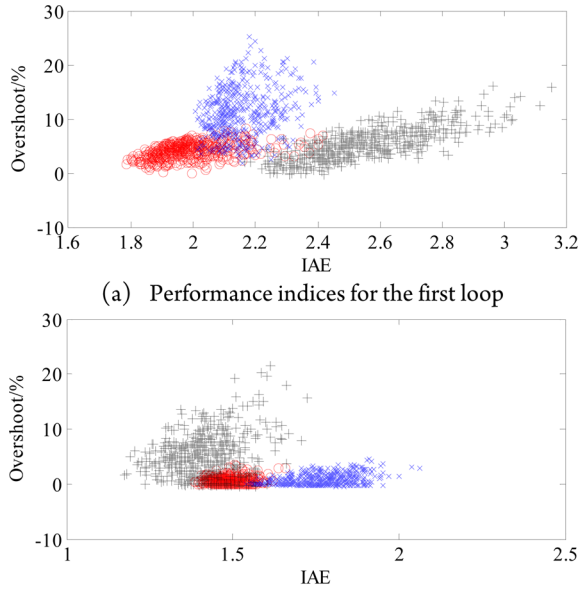

Figure 12. Results of the randomly perturbed plants for example 1 (+ centralized PI; × centralized PID; ○ ID-ADRC).

Table 1. Comparison of IAE for Example 2[a]

	IAE_1	IAE_2	sum
decentralized PI	8.31	21.46	29.77
decentralized ADRC	5.00	10.97	15.97
SD-PI	6.09	13.27	19.36
AD-PID	11.09	14.81	25.90
ID-ADRC (proposed)	**4.45**	**11.14**	**15.59**

[a] IAE_i represents the IAE for the ith loop

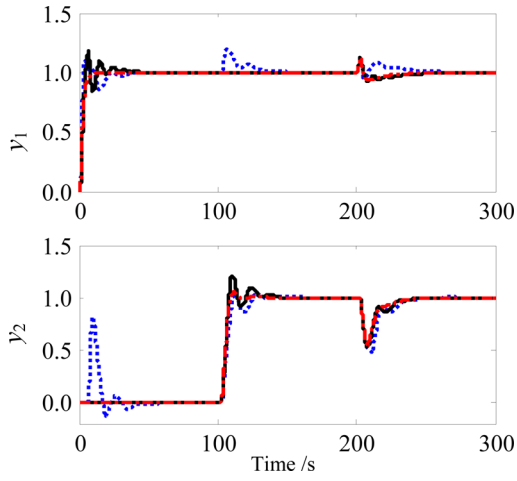

Figure 13. Tracking and disturbance rejection performance for example 2 (dotted in blue PI; dashed in black SD-PI; solid in red ID-ADRC).

5.3. Example 3. In this example, the process with a single RHP zero in a diagonal element is formulated

$$G(s) = \begin{bmatrix} \dfrac{e^{-12s}}{20s+1} & -\dfrac{2e^{-15s}}{(30s+1)^2} \\ \dfrac{e^{-17s}}{(40s+1)^2} & -\dfrac{3(5s-1)e^{-10s}}{(10s+1)^2} \end{bmatrix} \tag{41}$$

DOI: 10.1021/acs.iecr.5b03738
Ind. Eng. Chem. Res. 2016, 55, 2008−2019

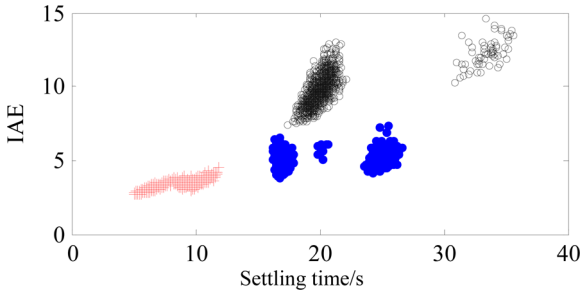

Figure 14. Results of the randomly perturbed plants for example 2 (● decentralized PI; ○ SD-PI; + ID-ADRC).

For this process, adjoint transfer matrix based decoupling[11] is applicable and will be compared with the ID-ADRC scheme, whose parameters are $b_{01} = 1.2$, $k_{p1} = 0.06$, $\omega_{o1} = 1.7$ for the first loop and $b_{02} = 1.3$, $k_{p2} = 0.21$, $\omega_{o2} = 0.11$ for the second loop. Also, decentralized PI parameters are obtained based on the genetic optimization method in ref 43. The nominal simulation and robustness tests are carried out with the same procedure as that in example 2. The results are shown in Figures 15 and 16. It is

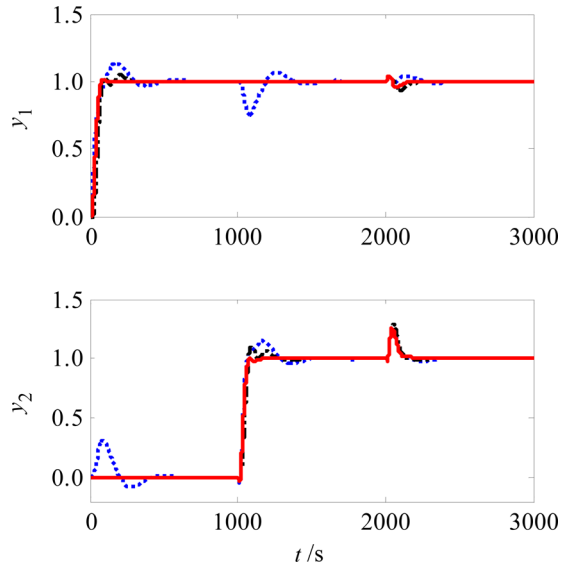

Figure 15. Tracking and disturbance rejection performance for example 3 (dotted in blue decentralized PI; dashed in black AD-PI; solid in red ID-ADRC).

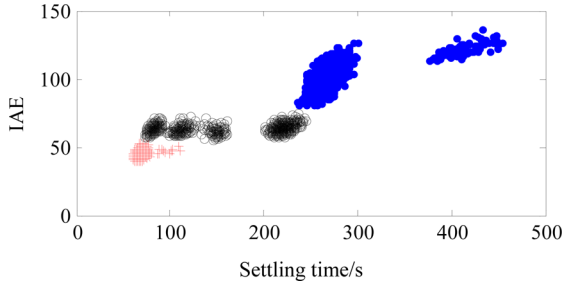

Figure 16. Results of the randomly perturbed plants for example 3 (● decsentralized PI; ○ SD-PI; + ID-ADRC).

seen that a perfect decoupling is obtained under ID-ADRC although it is derived from the Maclaurin approximation. And the robustness of ID-ADRC is much better than that of the AD-PI. These merits should be attributed to the compensation ability of ADRC.

5.4. Example 4. Consider the 4 × 4 HVAC process[46]

$$G(s) = \begin{bmatrix} \frac{-0.098e^{-17s}}{122s+1} & \frac{-0.036e^{-27s}}{(23.7s+1)^2} & \frac{-0.014e^{-32s}}{158s+1} & \frac{-0.017e^{-30s}}{155s+1} \\ \frac{-0.043e^{-25s}}{147s+1} & \frac{-0.092e^{-16s}}{130s+1} & \frac{-0.011e^{-33s}}{156s+1} & \frac{-0.012e^{-34s}}{157s+1} \\ \frac{-0.012e^{-31s}}{153s+1} & \frac{-0.016e^{-34s}}{151s+1} & \frac{-0.102e^{-16s}}{118s+1} & \frac{-0.033e^{-26s}}{146s+1} \\ \frac{-0.013e^{-32s}}{156s+1} & \frac{-0.015e^{-31s}}{159s+1} & \frac{-0.029e^{-25s}}{144s+1} & \frac{-0.108e^{-18s}}{128s+1} \end{bmatrix} \quad (42)$$

To handle the strong coupling in (42), Shen, Cai, and Li[46] designed a normalized decoupling based PI control (ND-PI) and Garrido, Vázquez, and Morilla[18] proposed an inverted decoupling based PI control (ID-PI). Based on the diagonal elements, decentralized ADRC and ID-ADRC are designed with the parameters shown in Table 2. The tracking performance is shown in Figure 17. The IAE of each loop is summarized in

Table 2. ADRC Parameters for Example 4

loop	ADRC parameters		
1st	$b_{01} = -0.075$,	$\omega_{c1} = 0.020$,	$\omega_{o1} = 7.5$
2nd	$b_{02} = -0.065$,	$\omega_{c2} = 0.022$,	$\omega_{o2} = 7.5$
3th	$b_{03} = -0.075$,	$\omega_{c3} = 0.022$,	$\omega_{o3} = 7.5$
4th	$b_{04} = -0.075$,	$\omega_{c4} = 0.020$,	$\omega_{o4} = 7.2$

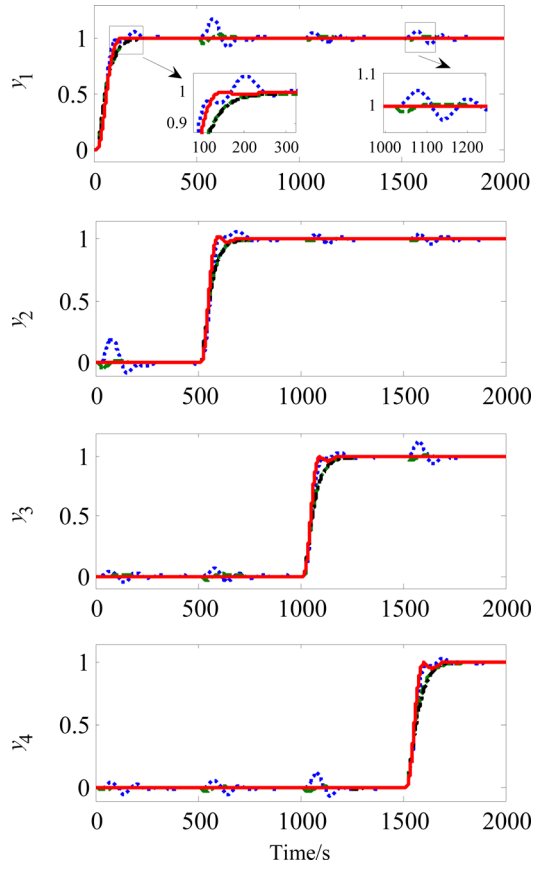

Figure 17. Tracking performance for example 4 (dotted in blue decentralized ADRC; dashed in green ND-PI; dashed−dotted in black ID-PI; solid in red ID-ADRC).

DOI: 10.1021/acs.iecr.5b03738
Ind. Eng. Chem. Res. 2016, 55, 2008−2019

Table 3. Comparison of IAE for Example 4

method	IAE_1	IAE_2	IAE_3	IAE_4
ADRC	93.92	93.54	85.86	90.77
ND-PI	76.03	73.67	76.86	78.98
ID-PI	69.44	67.85	70.67	79.96
ID-ADRC	**63.79**	**68.10**	**60.23**	**64.02**

Table 3. Again, ID-ADRC scheme obtains the best performance, demonstrating that the decentralized ADRC with inverted decoupling achieves better decoupling performance than the decentralized ADRC alone.

Disturbance rejection is rarely taken into explicit consideration in current decoupling literatures. Here, a unit step disturbance is added in the input of the first loop at t = 100 s and removed at t = 1000 s. The accelerated disturbance responses, shown in Figure 18, justify the merits of ADRC.

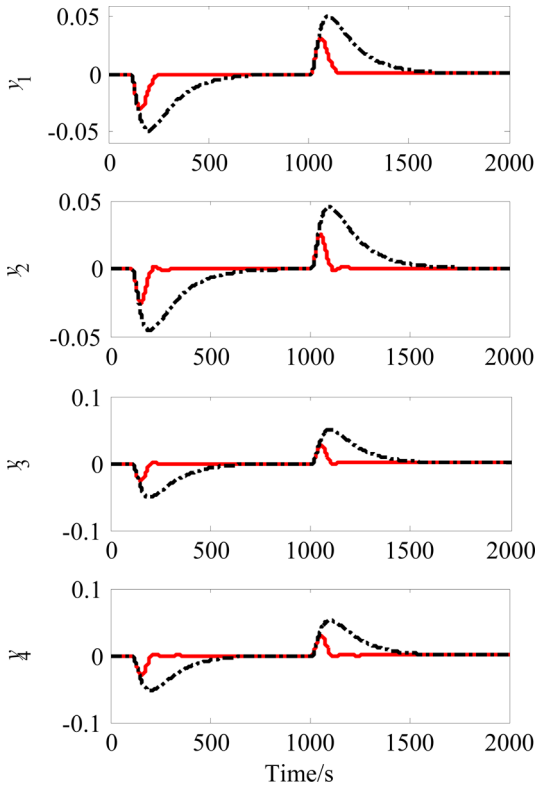

Figure 18. Disturbance performance for example 4. (black ID-PI; red ID-ADRC).

Finally, the tracking simulation for the step reference in the first loop is carried out for 1000 randomized systems with the ±10% perturbed parameters. The sum of IAE of the four loops and the settling time of the first loop are recorded in Figure 19. The scattered points demonstrate the overwhelming ability of ID-ADRC against modeling uncertainties.

5.5. Experimental Test. To further test the practicability of the combination of ADRC and inverted decoupling, the quadruple-tank level control system is tested, as depicted in Figure 20.

The controlled variables are the water levels of the lower tanks and the manipulated inputs are the voltages of the pump motors which transport the water to the upper tanks. The upper two tanks are linked via a communicating pipe, which brings couplings to the control loops.

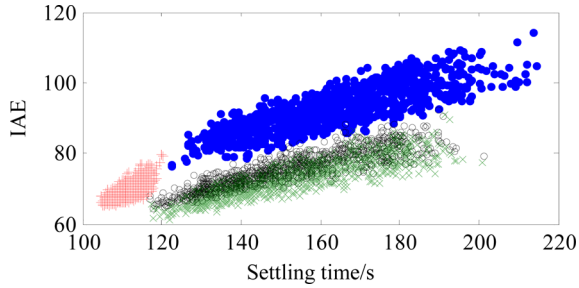

Figure 19. Results of the randomly perturbed plants for example 4 (● decentralized ADRC; ○ ND-PI; × ID-PI; + ID-ADRC).

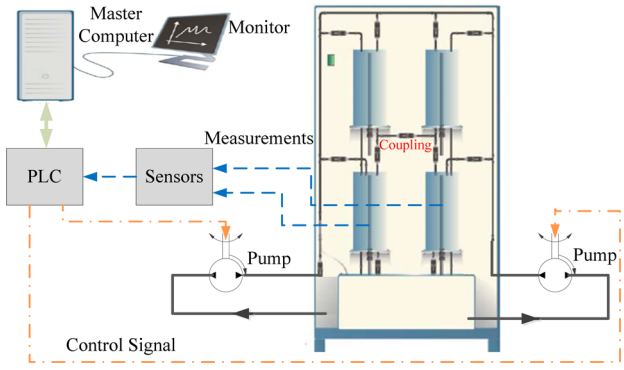

Figure 20. Quadruple-tank level control system.

On the basis of the linearized model around steady state, the decentralized PI, simplified decoupling based PI are designed based on the literatures and the inverted decoupling are designed based ADRC, with the results shown in Figure 21. This confirms that the proposed strategy is usable and achieves the fastest tracking and lowest coupling effects.

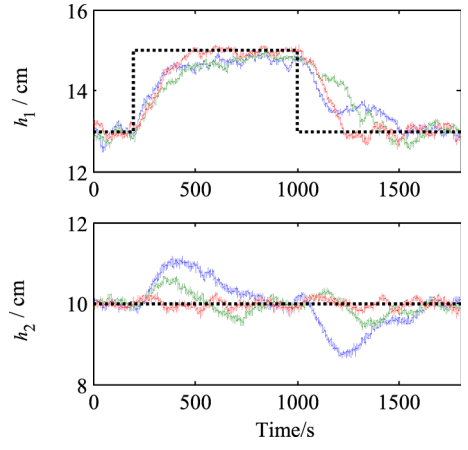

Figure 21. Tracking performances under different strategies (black setpoint; blue PI; green SD-PI; red ID-ADRC).

6. CONCLUSION AND FUTURE RESEARCH

It should be argued that the idea proposed in this paper is simple but it suggests a promising alternative for industrial multivariable control. Both the decoupler and the controller are engineering friendly, which can be realized in the DCS platform and with bumpless transfer. The modeling uncertainties are treated outside of the decoupler by ADRC. The simulation and experimental results demonstrate that the dynamic decoupling can be realized

DOI: 10.1021/acs.iecr.5b03738
Ind. Eng. Chem. Res. 2016, 55, 2008−2019

with better robustness. Furthermore, a better tracking and regulation performance is obtained compared with conventional schemes. Along the research line, the model information on the diagonal elements will be incorporated into the design of ADRC, either in terms of upgrading the interactive tuning tool for the model-based automatic computation and tuning, or in terms of embedding the model into ESO and ADRC to further improve its performance for single-loop and multivariable processes.

■ ASSOCIATED CONTENT

Supporting Information

The Supporting Information is available free of charge on the ACS Publications website at DOI: 10.1021/acs.iecr.5b03738.

Execute file, code files, and instructions for the robust interactive tuning tool for ADRC (ZIP)

Configuration diagram of the ADRC control logics based on the Ovation Distributed Control System, which incorporates the bumpless transfer block and can be directly utilized in industry (TIF)

■ AUTHOR INFORMATION

Corresponding Author

*E-mail: dongjy.thu@gmail.com.

Notes

The authors declare no competing financial interest.

■ ACKNOWLEDGMENTS

Research supported by National Natural Science Foundation of China (No. 51176086). The first author would like to give thanks to the China Scholarship Council (CSC), Grant 201406210142, for funding towards research at Baylor University.

■ REFERENCES

(1) Wu, X.; Shen, J.; Li, Y.; Lee, K. Y. Steam power plant configuration, design, and control. *Wiley Interdisciplinary Reviews: Energy and Environment* **2015**, *4*, 537.

(2) Lee, J. H. Model predictive control: review of the three decades of development. *International Journal of Control, Automation and Systems* **2011**, *9*, 415−424.

(3) Skogestad, S.; Postlethwaite, I. *Multivariable feedback control: Analysis and Design*; Wiley: London, 1996.

(4) Liu, T.; Zhang, W.; Gu, D. Analytical design of decoupling internal model control (IMC) scheme for two-input-two-output (TITO) processes with time delays. *Ind. Eng. Chem. Res.* **2006**, *45* (9), 3149−3160.

(5) Liu, T.; Zhang, W.; Gao, F. Analytical two-degrees-of-freedom (2-DOF) decoupling control scheme for multiple-input-multiple-output (MIMO) processes with time delays. *Ind. Eng. Chem. Res.* **2007**, *46* (20), 6546−6557.

(6) Liu, T.; Zhang, W.; Gao, F. Analytical decoupling control strategy using a unity feedback control structure for MIMO processes with time delays. *J. Process Control* **2007**, *17* (2), 173−186.

(7) Luyben, W. L. Distillation decoupling. *AIChE J.* **1970**, *16* (2), 198−203.

(8) Waller, K. V. T. Decoupling in distillation. *AIChE J.* **1974**, *20* (3), 592−594.

(9) Ogunnaike, B. A.; Ray, W. H. *Process dynamics, modeling, and control*; Oxford University Press: New York, 1994.

(10) Jin, Q. B.; Liu, Q. Decoupling Proportional−Integral−Derivative Controller Design for Multivariable Processes with Time Delays. *Ind. Eng. Chem. Res.* **2014**, *53* (2), 765−777.

(11) Shen, Y.; Sun, Y.; Li, S. Adjoint transfer matrix based decoupling control for multivariable processes. *Ind. Eng. Chem. Res.* **2012**, *51* (50), 16419−16426.

(12) Cai, W. J.; Ni, W.; He, M. J.; Ni, C. Y. Normalized decoupling: A new approach for MIMO process control system design. *Ind. Eng. Chem. Res.* **2008**, *47* (19), 7347−7356.

(13) Shinskey, F. G. *Process-control systems: application, design, adjustment*; McGraw-Hill Press: New York, 1988.

(14) Wade, H. L. Inverted decoupling: a neglected technique. *ISA Trans.* **1997**, *36* (1), 3−10.

(15) Garrido, J.; Vázquez, F.; Morilla, F.; et al. Practical advantages of inverted decoupling. *Proceedings of the Institution of Mechanical Engineers, Part I: Journal of Systems and Control Engineering* **2011**, *225* (7), 977−992.

(16) Garduno-Ramirez, R.; Lee, K. Y. Compensation of control-loop interaction for power plant wide-range operation. *Control engineering practice* **2005**, *13* (12), 1475−1487.

(17) Chen, P.; Zhang, W. Improvement on an inverted decoupling technique for a class of stable linear multivariable processes. *ISA Trans.* **2007**, *46* (2), 199−210.

(18) Garrido, J.; Vázquez, F.; Morilla, F. An extended approach of inverted decoupling. *J. Process Control* **2011**, *21* (1), 55−68.

(19) Garrido, J.; Vázquez, F.; Morilla, F. Centralized inverted decoupling control. *Ind. Eng. Chem. Res.* **2013**, *52* (23), 7854−7866.

(20) Garrido, J.; Vázquez, F.; Morilla, F. Inverted decoupling internal model control for square stable multivariable time delay systems. *J. Process Control* **2014**, *24* (11), 1710−1719.

(21) Åström, K. J.; Hägglund, T. *Advanced PID control*; ISA Press Research: Triangle Park, NC, 2006.

(22) Dong, J.; Sun, L.; Li, D.; Lee, K. Y.; Wu, Z. Inverted decoupling based active disturbance rejection control for multivariable systems. In *Proceedings of the 54th IEEE conference on decision and control*; IEEE Press: Osaka, Japan, 2015; pp 7353−7358.

(23) Han, J. From PID to active disturbance rejection control. *IEEE transactions on Industrial Electronics* **2009**, *56* (3), 900−906.

(24) Wu, D.; Chen, K. Frequency-Domain Analysis of Nonlinear Active Disturbance Rejection Control via the Describing Function Method. *IEEE Transactions on Industrial Electronics* **2013**, *60* (9), 3906−3914.

(25) Li, D.; Li, Z.; Gao, Z.; Jin, Q. Active Disturbance Rejection-Based High-Precision Temperature Control of a Semibatch Emulsion Polymerization Reactor. *Ind. Eng. Chem. Res.* **2014**, *53* (8), 3210−3221.

(26) Li, S.; Li, J.; Mo, Y. Piezoelectric multi-mode vibration control for stiffened plate using ADRC-based acceleration compensation. *IEEE Transactions on Industrial Electronics* **2014**, *61* (12), 6892−6902.

(27) Tian, G.; Gao, Z. Benchmark tests of active disturbance rejection control on an industrial motion control platform. In *Proceedings of American Control Conference*; IEEE, 2009; pp 5552−5557.

(28) Wu, D.; Chen, K. Design and analysis of precision active disturbance rejection control for noncircular turning process. *IEEE Transactions on Industrial Electronics* **2009**, *56* (7), 2746−2753.

(29) Huang, Y. Active disturbance rejection control: Methodology, practice and analysis. Presented at the *33rd Chinese Control Conference (CCC)*, Nanjing, China, July 28−30, 2014; http://tcct.amss.ac.cn/newsletter/2014/201408/images/Huang.pdf.

(30) Huang, C. E.; Li, D.; Xue, Y. Active disturbance rejection control for the ALSTOM gasifier benchmark problem. *Control Engineering Practice* **2013**, *21* (4), 556−564.

(31) Zhao, D.; Li, D.; Wang, Y. A Novel Boundary Control Solution for Unstable Heat Conduction Systems Based on Active Disturbance Rejection Control. *Asian Journal of Control* **2015**, DOI: 10.1002/asjc.1117.

(32) Zheng, Q.; Chen, Z.; Gao, Z. A practical approach to disturbance decoupling control. *Control Engineering Practice* **2009**, *17* (9), 1016−1025.

(33) Gao, Z. Scaling and bandwidth-parameterization based controller tuning. In *American Control Conference*, Denver, CO, June 4−6, 2003.

(34) Zheng Q.; Gao L.; Gao Z. On stability analysis of active disturbance rejection control for nonlinear time-varying plants with unknown dynamics. In *Proceedings of the IEEE Conference on Decision and Control*, New Orleans, LA, Dec 12−14, 2007; pp 12−14.

DOI: 10.1021/acs.iecr.5b03738
Ind. Eng. Chem. Res. 2016, 55, 2008−2019

(35) Zhao, C.; Li, D. Control design for the SISO system with the unknown order and the unknown relative degree. *ISA Trans.* **2014**, *53* (4), 858−872.
(36) Zhou, K.; Doyle, J. C.; Glover, K. *Robust and optimal control*; Prentice Hall, NJ, 1996.
(37) Jin, Q. B.; Liu, Q. IMC-PID design based on model matching approach and closed-loop shaping. *ISA Trans.* **2014**, *53* (2), 462−473.
(38) Wang, C.; Li, D. Decentralized PID controllers based on probabilistic robustness. *J. Dyn. Syst., Meas., Control* **2011**, *133* (6), 061015.
(39) Wang, C.; Li, D.; Li, Z.; et al. Optimization of controllers for gas turbine based on probabilistic robustness. *J. Eng. Gas Turbines Power* **2009**, *131* (5), 054502.
(40) Zhang, Y.; Xue, Y.; Li, D.; Sun, L. Digital realization for position active disturbance rejection controller with bumpless switching function. In *Proceedings of the 2014 Chinese Control Conference (CCC)*; IEEE: Nanjing, China, 2014; pp 3680−3684.
(41) Chien, I.; Huang, H.; Yang, J. A Simple Multiloop Tuning Method for PID Controllers with No Proportional Kick. *Ind. Eng. Chem. Res.* **1999**, *38* (4), 1456−1468.
(42) Xiong, Q.; Cai, W. J.; He, M. J. Equivalent transfer function method for PI/PID controller design of MIMO processes. *J. Process Control* **2007**, *17* (8), 665−673.
(43) Wood, R. K.; Berry, M. W. Terminal composition control of a binary distillation column. *Chem. Eng. Sci.* **1973**, *28* (9), 1707−1717.
(44) Tian, L.; Li, D.; Huang, C. E. Decentralized controller design based on 3-order active-disturbance-rejection-control. In *Proceedings of the 10th World Congress on Intelligent Control and Automation (WCICA)*; IEEE, 2012; pp 2746−2751.
(45) Tavakoli, S.; Griffin, I.; Fleming, P. J. Tuning of decentralised PI (PID) controllers for TITO processes. *Control Engineering Practice* **2006**, *14* (9), 1069−1080.
(46) Shen, Y.; Cai, W.; Li, S. Normalized decoupling control for high-dimensional MIMO processes for application in room temperature control HVAC systems. *Control Engineering Practice* **2010**, *18* (6), 652−664.

DOI: 10.1021/acs.iecr.5b03738
Ind. Eng. Chem. Res. 2016, 55, 2008−2019